Published in final edited form as:
*J Phys Chem B*. 2009 March 26; 113(12): 3799–3805. doi:10.1021/jp807749f.

# Non-linear elasticity of stiff filament networks: Strain stiffening, negative normal stress, and filament alignment in fibrin gels

**Hyeran Kang**, **Qi Wen**, and **Paul A Janmey**
Department of Physics and Astronomy, Institute for Medicine and Engineering, University of Pennsylvania

**Jay X. Tang**
Department of Physics, Brown University

**Enrico Conti** and **Fred C. MacKintosh**
Department of Physics and Astronomy, Vrije Universiteit, 1081 HV Amsterdam, The Netherlands

## Abstract

Many biomaterials formed by crosslinked semiflexible or rigid filaments exhibit non-linear rheology in the form of strain-stiffening and negative normal stress when samples are deformed in simple shear geometry. Two different classes of theoretical models have been developed to explain this non-linear elastic response, which is neither predicted by rubber elasticity theory nor observed in elastomers or gels formed by flexible polymers. One model considers the response of isotropic networks of semiflexible polymers that have non-linear force-elongation relations arising from their thermal fluctuations. The other considers networks of rigid filaments with linear force-elongation relations in which non-linearity arises from non-affine deformation and a shift from filament bending to stretching at increasing strains. Fibrin gels are a good experimental system to test these theories because the fibrin monomer assembles under different conditions to form either thermally fluctuating protofibrils with persistence length on the order of the network mesh size, or thicker rigid fibers. Comparison of rheologic and optical measurements shows that strain stiffening and negative normal stress appear at smaller strains than those at which filament orientation is evident from birefringence. Comparisons of shear to normal stresses and the strain-dependence of shear moduli and birefringence suggest methods to evaluate the applicability of different theories of rod-like polymer networks. The strain-dependence of the ratio of normal stress to shear stress is one parameter that distinguishes semi-flexible and rigid filament models, and comparisons with experiments reveal conditions under which specific theories may be applicable.

## Introduction

A common feature of many biomaterials that distinguishes them from most synthetic soft materials is their highly non-linear viscoelasticity. For crosslinked biopolymer systems, such as those forming the extracellular matrix or the cytoskeleton, non-linearity is evident as a strongly increasing shear modulus at moderate strains and a large negative normal stress. These mechanical features are likely to be important for the function of some tissues, and therefore the design principles that control them are likely to be useful for development of synthetic biomimetic materials. The molecular structures underlying non-linear elasticity in biomaterials are generally related to the elongated rodlike or semiflexible filaments that form many biological tissues, and gels formed from purified extracellular matrix or cytoskeletal proteins exhibit strain stiffening qualitatively similar to that seen in whole tissues such as muscle and mesentery.

Several different recent theoretical models have been proposed to account for strain stiffening [1-9] and a model of semiflexible filament network predicts the negative normal stresses observed in some materials [10]. Which of these models is most applicable to a specific material depends on how flexible the filaments are compared to the mesh size of the networks. More precisely, if the persistence length of the filament is comparable to the mesh size or distance between crosslinks within the network, as it is for isotropic networks of F-actin or fibrin protofibrils, then strain stiffening emerges naturally from an entropic model that considers how the thermal fluctuations of semiflexible polymer are constrained as the end-to-end distance of filament segments between crosslinks changes when the sample is deformed [1,2,7-9], as sketched in Figure 1A. This entropic model, which assumes no changes in the protein structure until the filament is pulled nearly straight, accounts very well for the nonlinear stiffening of crosslinked networks containing polymers with persistence lengths on the order of 100s of nm to a few microns. However many biomaterials contain filaments or filament bundles with larger diameters and persistence lengths so large compared to the mesh size that they are better modeled as stiff rods. For this case, mainly enthalpic models which are based on the orientation and stretching of fibers, have been proposed to explain the nonlinear elasticity observed in experiments [3-6]. The basic idea of these models, illustrated in Figure 1B, is that stiff fibers are easier to bend than to stretch. At low strains, deformation is dominated by bending, but, as strain increases and the filaments align in the strain direction, a transition occurs from bending modes to stretching modes that leads to increased stiffness at increased strains. This latter model predicts that at strains where the samples stiffen, changes in the protein structure can be expected [11].

Comparison of theories with experimental data is complicated by the fact that polymers with different persistence lengths also differ biochemically and structurally, and therefore different non-linear behaviors are not easily related solely to differences in filament stiffness. The biopolymer fibrin, the product of polymerization of the protein fibrinogen after activation by the protease thrombin (the final reactants in blood coagulation) enables comparison of semi-flexible and stiff rod networks composed of the same material. At high ionic strength and pH 8.5 fibrin monomers assemble in a well characterized half-staggered arrangement to make semiflexible protofibrils of approximately 10 nm diameter and 500 nm persistence length [1]. Fibrin protofibrils form stable branches during assembly to create gels with very little mechanical loss [12]. Experimentally, at the relatively high concentrations required to measure normal stresses, these systems are likely to contain some small protofibril bundles with persistence length perhaps greater than the mesh size, but previous studies have shown good correspondence between their measured strain-stiffening and that predicted by a theory for semiflexible filaments [1].

Under physiological ionic conditions, (pH 7.4, [NaCl] = 0.45) protofibrils assemble into fibers by lateral interactions that involve both specific, relatively weak protein bonds and interactions with chloride ions [13]. Such fibers, which appear too straight in light micrographs to exhibit any significant thermal fluctuations have diameters of approximately 100 nm and contain dozens or hundreds of protofibrils. Gels can be formed by either protofibrils or fibers, to make so-called fine and coarse clots, respectively [14].

The Young's moduli of individual fibrin protofibrils and filaments have been measured by analyses of persistence lengths [1] and deflection by microscopic probes [15,16], to yield values of 4 MPa and 2 MPa, respectively. The similarity of Young's moduli for protofibrils and fibers implies that the protofibrils within the fiber do not slide during deflection, and so coarse and fine fibrin gels can be considered as approximately uniform cylinders of the same material and chemical properties but differing in stiffness due to differences in diameter.

Here we report rheological measurements of shear modulus and normal stresses at a range of strains in fibrin gels and compare their non-linear elastic response with optical measures of polarized light retardance to quantify alignment of filaments. The results for coarse fibrin gels are consistent with expectations from theories of rodlike filament networks and show a transition from semi-flexible to rigid rod characteristics as the fiber diameter and therefore the stiffness of the fibrin fibers increases.

## Experimental Methods

### Materials

Fibrinogen and thrombin were purified from Atlantic salmon blood plasma as previously described [17, 18]. Fibrinogen at concentrations ranging from 2 mg/ml to 9 mg/ml was polymerized by addition of 0.5 U/ml to 1 U/ml thrombin to achieve clotting times on the order of 5 minutes in either T7 buffer (50 mM Tris, 150 mM NaCl at pH 7.4) or T8 buffer (50 mM Tris, 150 mM NaCl at pH 8.5) to form coarse and fine clots, respectively.

### Rheology

The viscoelastic moduli (G', G") of fibrin gels were measured using a strain-controlled rheometer (RFS-III, Rheometrics) with 25 mm parallel-plate geometry. At all times, the edges of the gels between the two plates were covered with buffer and mineral oil to prevent evaporation. Adhesion to the titanium plates of the rheometer was confirmed by the absence of plastic deformation even at the maximal strains measured and the low mechanical loss, as quantified by the ratio of G"/G' of the samples. To obtain the raw waveforms of shear and normal stress, an oscillatory sinusoidal strain $\gamma = \gamma_0 \sin \omega t$ was applied to the fibrin gels at a fixed frequency (f = 1 Hz). The analog data of shear strain $\gamma$, shear stress $\sigma_S$, and normal stress $\sigma_N$ were collected from the rheometer, and then converted to the digital signals with a Vernier analog/digital converter. A step rate (strain rate = 0.01 $s^{-1}$) test on the fibrin gels was also done to measure the strain dependence of the shear and normal stress at both pH 7.4 and pH 8.5. For these tests, the fibrin samples were let sit between the plates during their polymerizations. Shear strain was then applied in a clockwise direction at a constant rate (0.01/s) while monitoring the shear and normal stress.

The MITLaos program was used for applying the large amplitude oscillatory shear (LAOS) strain analysis in which the total shear stress with its elastic contribution as a function of the oscillatory strain is obtained[19]. Briefly, total shear stress $\sigma_S$ as a function of shear strain is obtained by averaging the raw data for several cycles of oscillatory shear. The total shear stress, $\sigma_S$, is then decomposed into two parts: a pure elastic stress $\sigma'$, which is the contribution of elastic response, and a pure viscous stress $\sigma"$, which is the contribution of viscous response. Each of these two parts is then further decomposed into harmonic representations using Chebyshev polynomials of the first kind as basis functions. Only odd-harmonics is included in the decomposition, since the stress response is assumed to be of odd symmetry with respect to the shear strain. The first harmonics represents linear response. Non-linearity in the elasticity can then be evaluated by analyzing the relative amplitude of the higher harmonics to the first harmonics.

### Birefringence

A fibrin gel of thickness 330 μm was formed between two slide glasses within a shear cell. The slide glasses were coated before applying the sample with 1 mg/ml poly-Lysine to prevent the slippage of the gel. After polymerization was complete within ~1 hr, simple shear strain was applied at an average strain rate = 0.03 $s^{-1}$. While applying shear strain to the gel we confirmed no slippage by embedding micron-beads in the gel and noting no displacement of the beads on the glass surface. The birefringence of strained fibrin gel at

each step of applied strain was measured using a polarizing microscope (Nikon Eclipse 800) equipped with a liquid crystal universal compensator (LC-PolScope, Cambridge Research and Instrumentation, Woburn, MA)[20,21] and imaged by a standard CCD camera (MTI 300RC; Dage-MTI, Michigan, IN) with 640 × 480 resolution. The LC-PolScope software measures the optical retardance and orientation of the slow axis at each pixel, thus providing the information on the local alignment of filaments.

## Results

### Theory

Two different models of crosslinked filament networks are considered. The first assumes that the filaments between crosslinks are elongated but semi-flexible and undergo thermal fluctuations that resist changes in the of end-to end distance because of increased configurational entropy. The second models the filaments as elastic rods that bend and stretch, but do not exhibit significant thermal fluctuations.

Following Ref. [2], we model a single semiflexible polymer segment of arclength $L$ with an energy given by

$$E=\int_0^L \left(\tfrac{1}{2}\kappa\left|\nabla^2 u\right|^2+\tfrac{1}{2}\tau|\nabla u|^2\right)dx$$

where $\kappa=k_B T\ell_p$ is the bending rigidity, $\ell_p$ is the persistence length, and $\tau$ is the tension in the filament. Here, $u(x)$ represents the transverse displacement of the filament, *e.g.*, relative to the line between the endpoints. For a filament in solution there are actually two independent directions in which it can fluctuate relative to the end-to-end line. We assume that these transverse deflections are the only degrees of freedom. For a stiff segment, for which $L$ is much less than $\ell_p$, the rod is nearly straight, and we will not distinguish between the contour length of the filament segment $L_c$ and the end-to-end distance $L$. We can, however, calculate the (small) difference $\Delta\ell=L_c-L$ using the integral

$$\Delta\ell=\int_0^L \tfrac{1}{2}|\nabla u|^2 dx$$

The integrals above can be done by a Fourier decomposition of the chain conformation into bending modes accounting for the two independent directions for filament deflections relative to the line between the ends. This leads to a calculation for the thermal average or equilibrium endto-end distance as a function of tension $\langle\Delta L(\tau)\rangle$, about which there will be thermal fluctuations, where the total energy in each of the bending modes is $\frac{1}{2}k_B T\ell_p$ on average. The *extension* relative to the equilibrium length at zero tension can be calculated analytically, and can be numerically inverted to yield the force/tension $\tau(\delta\ell)$ as a function of extension $\delta\ell$. This relation is shown in Figure 2a.

From this force-extension relation, the shear stress can be obtained for a given strain $\gamma$, assuming that the strain is small and uniform (affine) [1,2,7,22,23], as these results in stretching of filaments in the way sketched in Figure 1(a). If the shear is in the $x$-direction, for a filament with an orientation given by the usual polar angle $\theta$ (relative to the $z$-axis) and azimuthal angle $\phi$ (relative to the $x$-axis), the contribution to the shear stress for such a filament under tension is $\sin(\theta)\cos(\phi)\tau$. In a shear plane, however, there is a number density of these filaments given by $\cos(\theta)\rho$, where $\rho$ is the density of chains measured in length per unit volume. The tension also depends on the orientation of the chain segment, since the extension of the chain is given by $\delta\ell=\gamma L\cos(\phi)\sin(\theta)\cos(\theta)$. We assume that the network

consists of randomly and uniformly distributed rods of all orientations. Thus, the shear stress is given by the integral (over all angles $0 \leq \theta \leq \pi$ and $0 \leq \phi \leq 2\pi$)

$$\sigma_S = \int \sin(\theta)\cos(\theta)\cos(\phi)\,\tau\left[\gamma L \sin(\theta)\cos(\theta)\cos(\theta)\right]\sin(\theta)\,d\theta d\phi.$$

The calculation for the thrust as measured by the rheometer is similar, except that it is the z-component of tensioncos($\theta$)$\tau$, resulting in the integral

$$\sigma_N = \int \cos(\theta)\cos(\theta)\,\tau\left[\gamma L \sin(\theta)\cos(\theta)\cos(\phi)\right]\sin(\theta)\,d\theta d\phi.$$

This is sufficient to calculate the thrust only in the quasi-static (zero frequency) limit, since there will also be a non-zero component of the tension in the x-direction, i.e., in the direction of shear. Ordinarily this also contributes to the measured thrust. This gives, for instance, hoop stresses in a cone-and plate rheometer. These hoop stresses are balanced by a radial pressure gradient in incompressible samples, resulting in a positive contribution to the thrust. The relative openness of biopolymer gels, however, means that these hoop stresses can relax more quickly than for denser flexible gels. Our calculations here are for the quasi-static or zero frequency limit.

For small strains, both shear and normal stress are expected to be analytic in strain, meaning that they can each be approximated by a power series in strain. The two types of stress, however, have different symmetries with respect to strain. The shear stress changes sign with a change in sign of the strain, while the normal stress must be independent of the sign of the applied strain: the sample, for instance, should tend to contract upon twisting the rheometer plate in either direction. Thus, the shear stress must be a series of only odd powers of strain, with a dominant linear relationship between stress and strain for small values of strain. The normal stress, by contrast, can be expressed as a series of even powers, with a leading quadratic relationship between the thrust and the applied strain.

The calculated shear stress $\sigma_S$ and normal stress $\sigma_N$ above exhibit these properties. We find that the normal component $\sigma_N$ is always negative. Thus, in Figure 2b, we plot the ratio $-\sigma_N/\sigma_S$ versus strain $\gamma$. We observe a linear relationship or small stress, corresponding to the expected $\sigma_N \sim \gamma^2$ and $\sigma_S \sim \gamma$ behavior for small strain. Surprisingly, we find that $\sigma_N \cong -\sigma_S$ for larger strains (stresses). This can be understood qualitatively in terms of Figure 1a [10], where the stress is dominated by filaments oriented near 45 degrees with respect to shear. Such filaments contribute approximately equally to shear and normal stresses and the latter are strictly negative.

The model derived above is based on thermally fluctuating filaments. When the filaments become sufficiently rigid, it is no longer expected that their response to stress will be governed primarily by thermal fluctuations. In order study this regime; we have also performed numerical simulations of athermal elastic rods similar to Refs. [3, 24-26]. Here, initially isotropic and random networks of elastic rods are formed at different densities (measured in terms of the ratio of filament length to mean distance between cross-links, $L/\ell_c$) and with varying filament bending stiffness $\kappa$ and stretch modulus $\mu$. In addition to the shear stress, we have also computed the normal stress, and examined its dependence on network parameters, such as the filament stiffness[27].

As with the thermal networks discussed above, we also find that these athermal networks very generally exhibit negative normal stresses, although both the magnitude of these stresses and the onset of large normal stresses with increasing strain depend on the filament

stiffness. In Figure 3, we again plot the ratio $-\sigma_N/\sigma_S$ versus strain $\gamma$. We find three general features. Firstly, as for the thermal model above, the magnitudes of shear and normal stresses become comparable for strains larger than some threshold strain. However, in contrast with the thermal model, we find that the normal stresses can become substantially larger in magnitude than the shear stresses when filaments are more flexible to bending. We also find that the large normal stresses tend to develop at lower strains for more flexible systems, which can be understood in terms of the tendency of such filaments to buckle [3, 27, 28]. This is different from thermal networks, in which case the critical strain tends to increase with filament flexibility.

## When deformed in simple shear, gels formed by thick fibrin fibers exhibit both strain-stiffening in shear stress and a negative normal stress

The shear stress and normal stress resulting from a sinusoidal shear strain in the non-linear range for fibrin are shown in Figure 4a. As also observed in other biopolymer gels, the form of the shear stress deviates significantly from a simple sinusoidal response, with the peak maxima characteristic of shear-stiffening materials. The normal stress oscillates at twice the frequency of the shear strain and is negative at all strain magnitudes. In Figure 4b, the total shear stress $\sigma_S$ obtained by averaging raw data for 8 cycles of oscillatory shear and the elastic component $\sigma'$ of the shear stress obtained by LAOS analysis are plotted as functions of shear strain. The viscoelastic response of fibrin gel leads to the Lissajous pattern in the curve for total shear stress. The nonlinear increase of $\sigma'$ with increasing strain indicates the non-linear elasticity of fibrin gel. This non-linear stress response complicates the analysis of viscoelasticity from commercial rheometer software that typically assume linear response. The non-linear elasticity in oscillatory shear deformations can be evaluated in two ways; one is from the reading of the peaks in stress curves such as those in Figure 4a middle, the other from LAOS analysis[19,29] in which shear stress is plotted vs. shear strain from data averaged over multiple oscillatory cycles. The advantages and disadvantages of these methods to analyze oscillatory deformation in the non-linear range of strain amplitudes have recently been discussed in detail. An alternative method to measure nonlinear stress-strain responses is to apply a constant strain rate and measure the stress at successive intervals as the strain increases.

Figure 5a shows how the magnitude of both shear and normal stress increase with continuously increased strain. Networks of both fibrin protofibrils and thick fibrin fibers both exhibit increasingly large negative normal stresses as shear strain increases over a strain range where their shear moduli increase, and well any irreversible damage to the samples. The plot for the negative normal stress of the fibrin protofibril gel is consistent with that obtained in the previous studies of semiflexible polymer networks. In order to make quantitative comparisons of the magnitude of normal stress from semi-flexible and rigid polymer networks, Figure 5b shows the ratio of the magnitudes of negative normal stress to shear stress versus the applied strain for three different fibrin gels: one for pH 8.5 where the network strands are semiflexible ($L_p$ = 500 nm) and the other two for pH 7.4 where the networks strands are rigid ($L_p$ > 1 mm). As suggested by both models represented in Figure 1A and 1B, stretching and aligning of filaments under shear is expected to result in the most tensed filaments contributing nearly equally to both shear and normal stress. Thus, in the highly nonlinear regime, the shear and normal stress are expected to be of the same magnitude, with the latter being strictly negative, corresponding to contraction perpendicular to the shear direction.

The ratio of the magnitude of normal stress to shear stress increases to a maximum at small strains of about 10-20%, and then decreases at large strains for all three samples. This overshoot trend is more prominent for a the fibrin gel at pH 8.5, with flexible protofibrils, in comparison with two other gels at pH 7.4, that contain stiff fibers. Although previous studies

of fibrin gels made at pH 8.5 modeled these systems as purely semi-flexible polymers, ratios of normal to shear stress greater than 1 are inconsistent with a purely thermal model and suggest that even fine fibrin gels contain some strands, possible small protofibril bundles, that behave more as bending and stretching rods as depicted in Figure 3.

### Filament alignment, as measured by optical retardance increases with increasing shear strain but lags behind the increase in shear modulus

In order to quantify the filament alignment, we performed birefringence measurement using a polarizing microscope. Figure 6 shows the strain dependence of the average optical retardance overlaid with the shear moduli of 3 mg/ml human fibrin gel at pH 7.4. The optical retardance is defined as $(\Delta n \cdot d)$ , where $\Delta n$ is the difference in refractive index of a birefringent sample between its slow and fast axes and d is the distance of light path. The representative birefringent images taken at strain $\gamma = 0$, 0.3, 0.6 and 1.0 exhibit a correlated direction of polarization in the direction of the applied shear strain. The direction of the slow axis points along the direction of the applied shear strain, and the fast axis is perpendicular to both the slow axis and the direction of light propagation. The average retardance gradually increased from 0.5 nm up to 4.25 nm as the shear strain $\gamma$ continuously increased from 0 to 1.0 at a rate of 0.03 $sec^{-1}$. The onset point for the strain-stiffening is around $\gamma = 0.1$, obtained by noting the start of a rapid increase from the shear modulus plot. The optical retardance starts to increase rapidly at a higher strain value of $\gamma = 0.3$, indicating a lag of the filament alignment behind the increase of shear modulus.

The extent of alignment of filaments in a network, measured in the form of optical birefriengence, is proportional to the order parameter [30]. The range of the order parameter is from zero, for an isotropic sample without any alignment, to 1, when all constituent filaments are totally aligned. The results of our measurements shown in Figure 6 suggest that significant alignment of the fibrin filaments is caused by shear strain of 0.3 or higher. This result is qualitatively understandable by visualizing the act of shear deformation on an entangled and initially isotropic network. A quantitative explanation for the measured lag of order parameter behind the rise of the shear modulus requires, however, a computation of the order parameter as a function of the shear strain aided by modeling the network as illustrated in Figure 1. This particular calculation has not been performed for the system of fibrin networks yet.

## Discussion

Strong nonlinear mechanical response to strain and stress has been found to be a general feature of protein biopolymer networks. This has been most widely observed in the strong tendency of networks to stiffen under strain. More recently, it has also been shown that many of the same systems exhibit highly unusual negative normal stress [10, 31]. The general features of non-linear elasticity can be accounted for by two different models that represent different limits of filament stiffness and network density. These models make different assumptions about filament flexibility and the role of thermal fluctuations. Strain stiffening and negative normal stress arises inevitably for isotropic crosslinked networks of thermally writhing semi-flexible filaments. In this model, an analytic calculation of the force extension relation for single filaments between network junctions leads to a non-linear macroscopic network response, in which individual filaments are soft to compression but become increasingly resistant to elongation. This model appears to describe the rheology of networks formed by relatively dilute fibrin protofibril gels, as well as crosslinked F-actin and intermediate filaments, for which the persistence length of the polymers is on the order of the network mesh size. Specifically, this model predicts both a decrease in the critical strain for the onset of nonlinear elasticity with increasing network density, as well as a rapid increase in stiffness with stress and strain, in agreement with experiment [2,7,8,10,32].

Other biopolymer gels, such as those composed of collagen or coarse fibrin fibers are unlikely to be adequately treated by such an entropic model for semiflexible polymers, because the fibers in these systems have bending moduli up to thousands of times higher and do not exhibit significant thermal fluctuations. Nevertheless, these systems also strain-stiffen and exert negative normal stress under shear deformation as shown in Figures 4 and 5. Here, an athermal model of interconnected elastic rods is likely more appropriate than one based on thermal fluctuations. In simulations, networks of elastic rods have been shown to exhibit nonlinear elasticity that arises from network geometric considerations that lead to a shift from bending to stretching of fibers as strain magnitude increases, even if the elasticity of single fibers is linear [3, 5]. More recent simulations show that such models can also lead to negative normal stresses [27, 33]. While both entropic and athermal, mechanical models can account for the nonlinear elastic response of biopolymer gels, the two models predict observable differences in detail.

The two theories have different predictions for several key rheological parameters. Specifically, the two models make different predictions for the onset, degree, and functional form of strain stiffening. For instance, the onset of nonlinearity in thermal simulations of elastic rods corresponds to buckling of filament segments, which tends to occur at larger strains in more concentrated networks [3,27,33,34]. The ratio of magnitudes of shear and normal stresses are also different. For instance, the purely thermal model does not allow the normal stress magnitude to exceed shear stress, whereas the athermal model does. The models also predict different dependences of normal stresses on frequency of oscillation or rate of strain, but experimental measurements of these effects have not yet been made. In real systems, it is probably unlikely that a material will behave only as one or the other of the two models. The boundary between semi-flexible and stiff may be blurred by heterogeneities in filament stiffness or crosslink distance, as suggested by the finding that most aspects of fine fibrin gels are well explained by the thermal model, but the large ratio of normal to shear stress is not. Whether this discordance reflects some limit to the theories or results from as yet uncharacterized contractile stresses that arise in the samples during gelation remains to be determined. Further experimental studies of crosslinked networks with known and variable filament stiffness are needed to evaluate the applicability of these different theories for specific biopolymer materials.

## Acknowledgments

This work was supported by NSF/MRSEC grant 05-20020 and NIH R01 GM083272.

## References

1. Storm C, Pastore JJ, MacKintosh FC, Lubensky TC, Janmey PA. Nature. 2005; 435:191. [PubMed: 15889088]
2. MacKintosh FC, Kas J, Janmey PA. Physical Review Letters. 1995; 75:4425. [PubMed: 10059905]
3. Onck PR, Koeman T, van Dillen T, van der Giessen E. Phys Rev Lett. 2005; 95:178102. [PubMed: 16383874]
4. Didonna B, Lubensky T. Physical Rev. E. 2005; 72:066619.
5. Huisman EM, van Dillen T, Onck PR, Van der Giessen E. Phys Rev Lett. 2007; 99:208103. [PubMed: 18233190]
6. Heussinger C, Bathe M, Frey E. Phys Rev Lett. 2007; 99:048101. [PubMed: 17678408]
7. Gardel ML, Shin JH, MacKintosh FC, Mahadevan L, Matsudaira P, Weitz DA. Science. 2004; 304:1301. [PubMed: 15166374]
8. Gardel ML, Shin JH, MacKintosh FC, Mahadevan L, Matsudaira PA, Weitz DA. Phys Rev Lett. 2004; 93:188102. [PubMed: 15525211]
9. Palmer JS, Boyce MC. Acta Biomater. 2008; 4:597. [PubMed: 18325860]

10. Janmey PA, McCormick ME, Rammensee S, Leight JL, Georges PC, MacKintosh FC. Nat Mater. 2007; 6:48. [PubMed: 17187066]
11. Brown AE, Litvinov RI, Discher DE, Weisel JW. Biophys J. 2007; 92:L39. [PubMed: 17172299]
12. Janmey PA, Amis E, Ferry J. J. Rheol. 1983; 27:135.
13. Di Stasio E, Nagaswami C, Weisel JW, Di Cera E. Biophys J. 1998; 75:1973. [PubMed: 9746538]
14. Ferry JD, Morrison PR. J. Am. Chem Soc. 1947; 69:388. [PubMed: 20292443]
15. Collet JP, Shuman H, Ledger RE, Lee S, Weisel JW. Proc Natl Acad Sci U S A. 2005; 102:9133. [PubMed: 15967976]
16. Guthold M, Liu W, Sparks EA, Jawerth LM, Peng L, Falvo M, Superfine R, Hantgan RR, Lord ST. Cell Biochem Biophys. 2007; 49:165. [PubMed: 17952642]
17. Michaud SE, Wang LZ, Korde N, Bucki R, Randhawa PK, Pastore JJ, Falet H, Hoffmeister K, Kuuse R, Uibo R, Herod J, Sawyer E, Janmey PA. Thromb Res. 2002; 107:245. [PubMed: 12479886]
18. Wang LZ, Gorlin J, Michaud SE, Janmey PA, Goddeau RP, Kuuse R, Uibo R, Adams D, Sawyer ES. Thromb Res. 2000; 100:537. [PubMed: 11152934]
19. Ewoldt RH, Hosoi AE, Mckinley GH. Ann. Trans. Nord. Rheol. Soc. 2007; 15:3.
20. Oldenbourg R, Salmon ED, Tran PT. Biophys J. 1998; 74:645. [PubMed: 9449366]
21. Shribak M, Oldenbourg R. Appl Opt. 2003; 42:3009. [PubMed: 12790452]
22. Gittes F, MacKintosh F. Phys. Rev. E. 1998; 58:R1241.
23. Morse D. Physical Review E. Statistical Physics, Plasmas, Fluids, & Related Interdisciplinary Topics. 1998; 58:R1237.
24. Head DA, Levine AJ, MacKintosh FC. Phys. Rev. Lett. 2003; 91:108103. [PubMed: 14525511]
25. Wilhelm J, Frey E. Phys. Rev. Lett. 2003; 91:108103. [PubMed: 14525511]
26. Head DA, Levine AJ, MacKintosh FC. Phys Rev E Stat Nonlin Soft Matter Phys. 2003; 68:061907. [PubMed: 14754234]
27. Conti E, MacKintosh F. arXiv:0807.1935. 2008
28. Heussinger C, Frey E. Phys Rev Lett. 2006; 96:017802. [PubMed: 16486518]
29. Cho KS, Hyun K, Ahn KH, Lee SJ. J.Rheol. 2005; 49:747.
30. Viamontes J, Narayanan S, Sandy AR, Tang JX. Physical Review E. 2006; 73:061901.
31. Wen Q, Basu A, Yodh JWA, Janmey P. New J Physics. 2007; 9:428.
32. Tharmann R, Claessens MM, Bausch AR. Phys Rev Lett. 2007; 98:088103. [PubMed: 17359131]
33. Heussinger C, Schaefer B, Frey E. Phys Rev E Stat Nonlin Soft Matter Phys. 2007; 76:031906. [PubMed: 17930270]
34. Heussinger C, Frey E. Phys Rev Lett. 2006; 97:105501. [PubMed: 17025825]

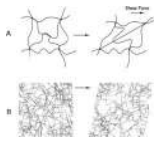

**Figure 1. Schematic diagram for two different mechanisms of strain stiffening**

(a) Semiflexible polymers linked at ends in network junctions lose configurational entropy as their end-to-end distances increase or decrease from their resting lengths during shear deformation. Filaments with intrinsically non-linear force elongation relations resist elongation more strongly the more they are stretched to the limit at which the end-to-end distance equals their contour length. Adapted from Ref. 2.

(b) Stiff filaments deform initially by bending at small strains and then by stretching at larger strains when their end-to-end vectors align in the shear field. In this mode, fibers with linear force-extension relations can also produce strain stiffening in networks because of the geometrical changes as they align in shear. Adapted from Ref. 3

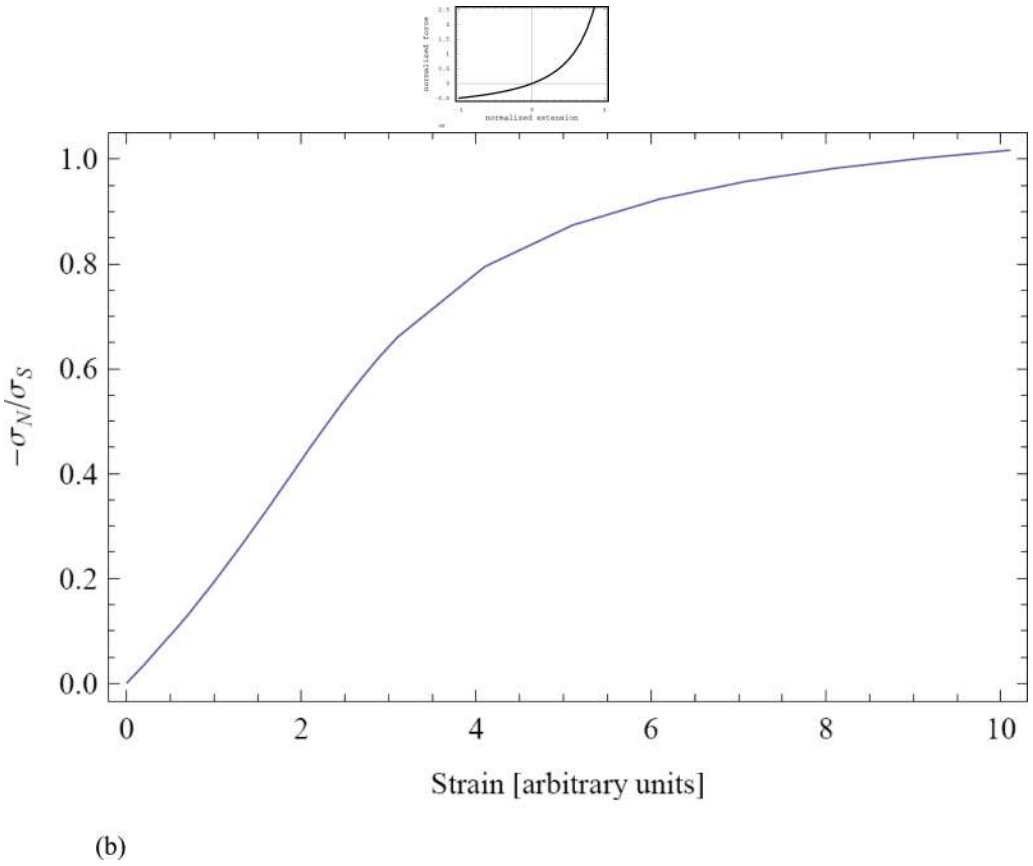


(b)

**Figure 2.**

(a) Normalized force-extension relation for a thermally fluctuating semi-flexible filament of length $L$ derived from the model of [1, 2]. Here, the force is in units of $\kappa\pi^2 / L^2$, and the strain is plotted as a multiple of $L/\pi^2\ell_p$. (b) The ratio of normal stress to shear stress as a function of shear strain (in arbitrary units) for isotropic crosslinked networks of filaments with the force-extension relation shown in Figure 2 (a).

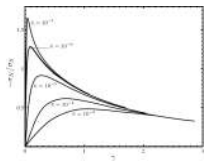

**Figure 3.**

The ratio of normal to shear stress versus applied strain $\gamma$ for constant density $L/\ell_c=15$ and various filament bending stiffnesses. Here, the bending modulus $\kappa$ is normalized by $\mu L^2$, where $\mu$ is the stretch modulus of a filament. On decreasing filament bending stiffness ($\kappa$) a peak grows, becoming more pronounced and moving to smaller strain. For large strain the curves depend weakly on κ, showing a regime dominated by stretching only. This can explain the slowly decreasing ratio at high strain, since filament alignment with the shear direction results in a reduced fraction of stress in the normal direction.

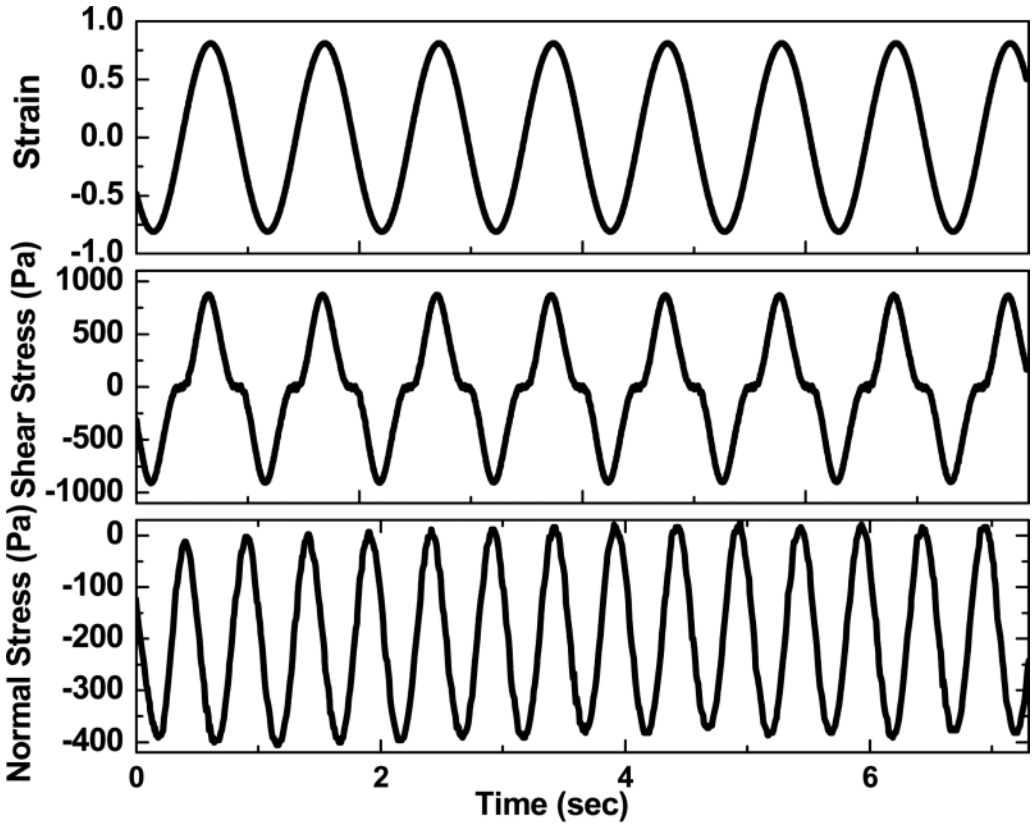


(a)

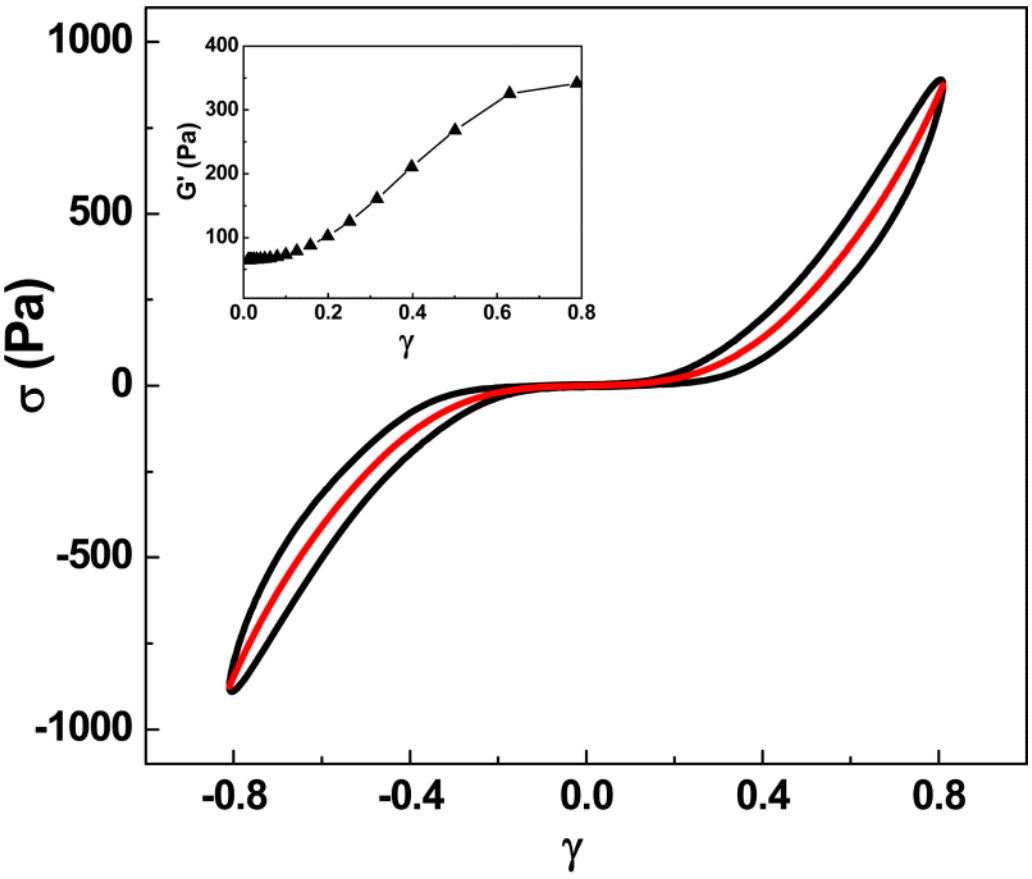


(b)

**Figure 4.**

(a) The raw waveforms of strain (top) and shear stress (middle) and normal stress (bottom) from the analog output of the Rheometrics RFS III instrument. The oscillatory strain (80 %) was applied to the fibrin gel at f = 1 Hz. The frequency doubling observed in the normal stress signal can be attributed to the fact that the normal stress does not depend on the shear directions. Sample condition: 2.5 mg/ml salmon fibrin gel at pH 7.4, and [NaCl] = 0.15 mM (b) The total shear stress (dark line) obtained from the raw data averaged over eight oscillatory cycles and the elastic component of shear stress (red solid single line) computed from large amplitude oscillatory shear (LAOS) analysis as functions of the oscillatory strain. (Inset) The shear modulus reported by rheometer software as a function of shear strain amplitude is plotted.

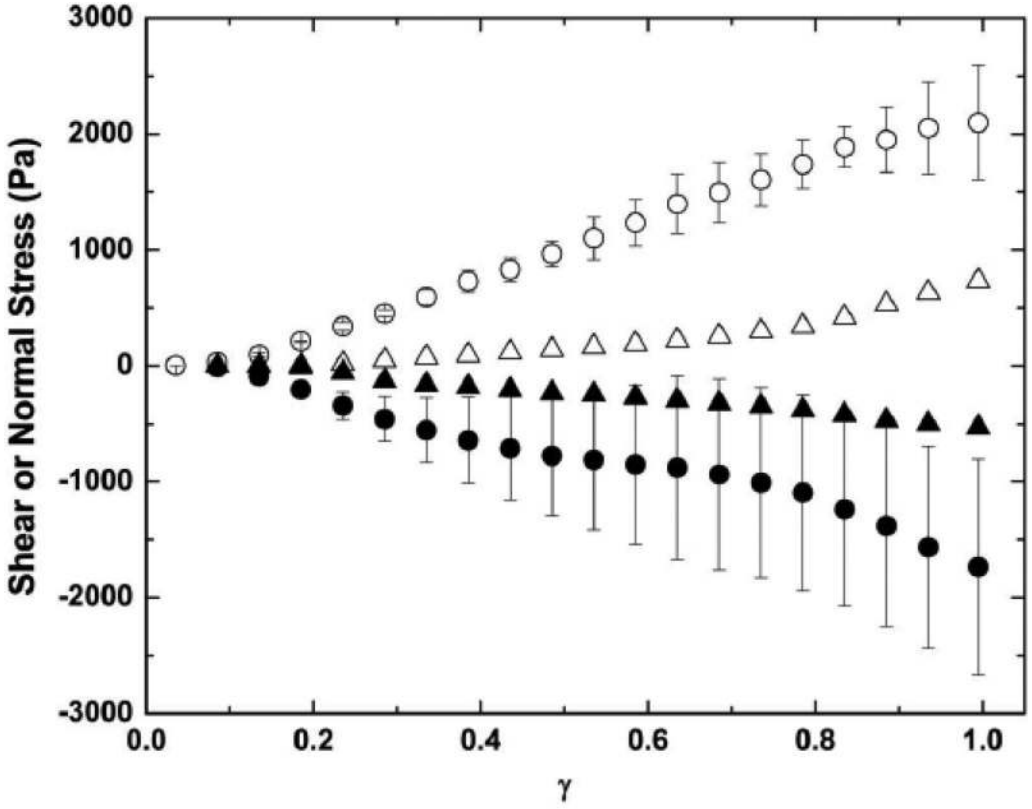


(a)

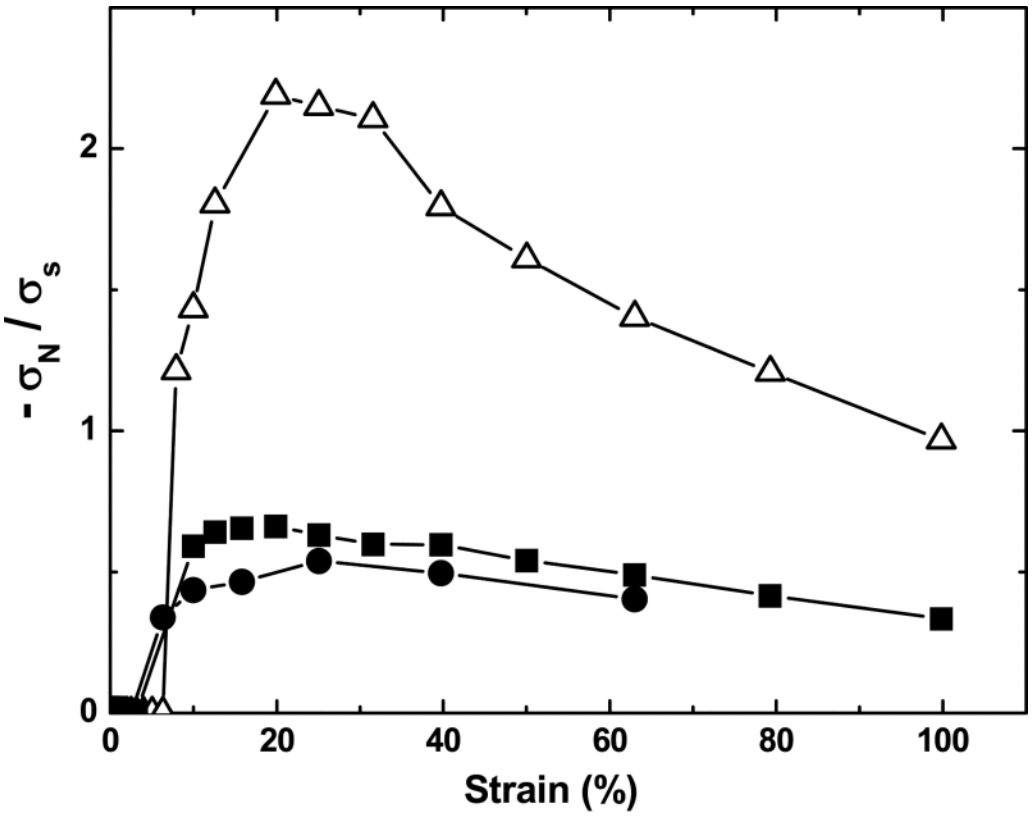


(b)

**Figure 5.**

(a) The both shear and negative normal stress are plotted versus constantly increasing strain (d γ/d t = 0.01 $s^{-1}$) for 2.5 mg/ml fibrin gels at pH 7.4 (open and solid circles) and pH 8.5 (open and solid triangles). The error bars for values at pH 7.4 were obtained by averaging three different samples.

(b) The ratio of the negative normal stress to the shear stress of fibrin gels is plotted against varying strains; 4.0 mg/ml salmon fibrin at pH 8.5 (open triangles), 4.0 mg/ml salmon fibrin at pH 7.5 (solid rectangles), and 6.0 mg/ml human fibrin at pH 7.5 (solid circles). Networks of more flexible protofibrils (pH 8.5) show a more prominent overshoot in comparison with coarse networks (pH 7.5) of stiffer filaments.

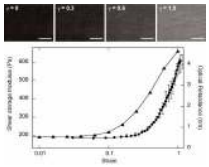

**Figure 6.**
Comparison of filament alignment with strain-stiffening. The average optical retardance (circles) increases with increased shear strain, but lags behind the increase in shear modulus (triangles) of the same sample. Sample preparation: human fibrin 3 mg/ml at pH 7.4. Above the plot are representative images takes at strain = 0, 0.3, 0.6, and 1.0 (left to right), showing increasing retardance magnitude (lightness) and correlated direction of polarization. The red lines indicate local slow axis orientations, which are increasingly aligned along the direction of applied shear strain. The scale bar represents 50 μm.